

# Work statistics of sudden Quantum quenches: A random matrix theory perspective on Gaussianity and its deviations.

Miguel Tierz<sup>1,\*</sup>

<sup>1</sup>*Shanghai Institute for Mathematics and Interdisciplinary Sciences  
Block A, International Innovation Plaza, No. 657 Songhu Road, Yangpu District,  
Shanghai, China*

(Dated: September 12, 2025)

We show that, for sudden quenches, the work distribution reduces to the statistics of the traces of powers of Haar unitaries, which are random unitary matrices drawn uniformly from the unitary group. For translation-invariant quadratic fermionic chains with interactions extending to  $m$  neighbors and periodic boundary conditions, the Loschmidt amplitude admits a unitary matrix model / Toeplitz representation, which yields a work variable of the form  $W = \sum_{r \leq m} a_r \Re \text{Tr } U^r$  (and in models with pairing terms -superconducting pairing- additional  $b_r \Im \text{Tr } U^r$  terms appear). By invoking multivariate central limit theorems for vectors of traces of unitaries, we obtain a Gaussian distribution for  $P(W)$  with variance  $\text{Var}(W) = \frac{1}{2} \sum_r r (a_r^2 + b_r^2)$  and asymptotic independence across different powers. We also characterise the conditions under which non-Gaussian tails arise, for example from many interaction terms or their slow decay, as well as the appearance of Fisher-Hartwig singularities. We illustrate these mechanisms in the XY chain. Various numerical diagnostics support the analytical results.

## I. INTRODUCTION

Understanding the statistics of *work* performed during rapid nonequilibrium protocols has become a central theme in quantum thermodynamics [1]. To define work we consider a protocol in which external controls  $\lambda(t)$  are varied during a time window  $t \in [0, \tau]$ . The system Hamiltonian is

$$H(t) \equiv H(\lambda(t)), \quad H_i := H(\lambda(0^-)), \quad H_f := H(\lambda(\tau^+)). \quad (1)$$

The term *drive* refers to the (possibly instantaneous) time dependence  $t \mapsto \lambda(t)$  on  $[0, \tau]$ , which generates the unitary

$$U_\tau = \mathcal{T} \exp \left( -i \int_0^\tau H(\lambda(t)) dt \right). \quad (2)$$

In the two-projective-measurement (TPM) scheme [1], one measures  $H_i$  at  $t = 0^-$ , evolves with  $U_\tau$ , and then measures  $H_f$  at  $t = \tau^+$ . If  $H_i |n^0\rangle = E_n^{(0)} |n^0\rangle$  and  $H_f |m^1\rangle = E_m^{(1)} |m^1\rangle$ , the work random variable is

$$w = E_m^{(f)} - E_n^{(i)}, \quad (3)$$

with probabilities  $p_n^{(0)} = \langle n^0 | \rho_0 | n^0 \rangle$  and  $p_{m|n} = |\langle m^1 | U_\tau | n^0 \rangle|^2$ . The characteristic function of work,

$$\chi_W(u) = \int_{\mathbb{R}} e^{iuw} P(w) dw, \quad (4)$$

has the standard operator form

$$\chi_W(u) = \text{Tr} \left( e^{iuH_f} U_\tau e^{-iuH_i} \rho_0 U_\tau^\dagger \right). \quad (5)$$

In a *sudden quench* [2] the drive is instantaneous at  $t = 0$ : we set  $\tau = 0^+$  and evolve for a time  $t$  under  $H_f$ . If the prepared state is an eigenstate  $H_i |\psi_0\rangle = E_0 |\psi_0\rangle$  (the usual situation in our applications; e.g. a translation-invariant ground state, or a domain-wall state chosen as the ground state of a simple  $H_i$ ), then (5) reduces to

$$\chi_W(u) = e^{-iuE_0} \langle \psi_0 | e^{iuH_f} | \psi_0 \rangle = e^{-iuE_0} G(-u), \quad (6)$$

where

$$G(t) := \langle \psi_0 | e^{-iH_f t} | \psi_0 \rangle \quad (7)$$

is the *Loschmidt amplitude*, and  $L(t) = |G(t)|^2$  the Loschmidt echo [2]. In the quadratic fermion models of interest, the problem can be mapped to a unitary matrix integral [3, 4]. Specifically, we will see that  $G(t)$  takes the form of a Toeplitz determinant, allowing us to interpret  $\chi_W(u)$  as a characteristic function of a random-matrix linear statistic. Toeplitz matrices are structured matrices, constant along diagonals, whose determinant is well-known to be equivalent to partition functions of unitary random matrix ensembles [5, 6]. Equation (6) is the precise content of the heuristic statement “the work characteristic function is the Loschmidt amplitude (up to a phase)” used throughout.

Thus  $P(w)$  is the Fourier transform of a Loschmidt-type object, while the familiar Loschmidt echo  $L(t) = |G(t)|^2$  quantifies the decay of fidelity after the quench [2, 7–11]. This Loschmidt amplitude and work statistics connection has driven much of the modern activity on *dynamical quantum phase transitions* (DQPTs), where nonanalytic features in  $G(t)$  govern far-from-equilibrium behavior [11, 12]. On the experimental side, interferometric protocols access  $\chi(u)$  directly via an ancilla, enabling reconstructions of  $P(w)$  and tests of fluctuation relations in a variety of platforms [13–15].

\* tierz@simis.cn

The key structural observation we develop and exploit is that, for sudden quenches in quadratic (or effectively free) spin or fermionic models with periodic boundary conditions (PBC) and finite-range couplings<sup>1</sup>, the Loschmidt amplitude admits a Toeplitz (or block-Toeplitz) determinant representation whose symbol is  $e^{iu\varepsilon(k)}$  [3, 4], where  $\varepsilon(k)$  is the single-particle dispersion of the post-quench Hamiltonian, expressed after the appropriate mode rotation when needed. This actually means the Loschmidt amplitude can be written as  $\det[T_N(\phi)]$  for some function (symbol)  $\phi(\theta) = e^{iu\varepsilon(\theta)}$ , whose Fourier coefficients are the elements of the structured matrix, constant along diagonals,  $T_N(\phi)$ . Expanding  $\varepsilon(k)$  in Fourier modes,

$$\varepsilon(k) = a_0 + \sum_{m \geq 1} (a_m \cos mk + b_m \sin mk), \quad (8)$$

and using Heine–Szegő-type identities [5], to be described below, the characteristic function can be written as an average over the unitary group,

$$\chi(u) = \mathbb{E}_{U(N)} \left[ \exp \left( iu \sum_{m \geq 1} (\alpha_m \text{Tr } U^m + \alpha_m^* \text{Tr } U^{-m}) \right) \right]. \quad (9)$$

with explicit coefficients  $\alpha_m$  determined by the quench and microscopic couplings.

In other words, *the logarithm of the characteristic function is the cumulant generating functional of a linear statistic of traces of powers of a Haar-distributed unitary*. This places  $P(w)$  squarely in the scope of classical and influential probabilistic results on traces of random unitary matrices: for fixed  $m$  as  $N \rightarrow \infty$ , the variables  $\{\text{Tr } U^m\}_{m \geq 1}$  converge jointly to independent complex Gaussians with

$$\mathbb{E}[\text{Tr } U^m] = 0, \quad \text{Var}(\text{Tr } U^m) = m, \quad (10)$$

and asymptotic independence across different  $m$  [16–18]. Recent multivariate refinements give super-exponential rates in total variation and quantify regimes where the number of included harmonics  $m$  may grow with  $N$  while retaining Gaussianity [19, 20]. This implies that if  $m$  is not too large relative to  $N$ , the Gaussian approximation holds extremely well.

Two points are worth emphasizing. First, the *normalization* here differs from the classical central limit theorem (CLT) for sums of weakly dependent random variables: there is no  $1/\sqrt{N}$ ; instead the intrinsic variance scale of  $\text{Tr } U^m$  is  $m$ , and Gaussianity emerges in the large- $N$  limit with  $m$  fixed (or  $m$  slowly growing) [16, 19]. Second, the

physics of microscopic couplings appears only through the weights  $\alpha_m$  multiplying the (asymptotically independent) Gaussian modes. As a consequence, to leading order the work distribution  $P(w)$  is Gaussian with zero mean shift determined by  $a_0$  and a variance

$$\text{Var}[w] = 2 \sum_{m \geq 1} m |\alpha_m|^2, \quad (11)$$

while controlled, model-specific non-Gaussian corrections arise from (i) including many harmonics  $m$  that grow with  $N$  beyond the proven CLT regime, and/or (ii) singular features in the symbol (e.g., Fisher–Hartwig-type discontinuities [5, 21]) that generate subleading cumulants. As a numerical check, the sample variance plateaus at the theoretical value in (11); see Fig. 1(a). The overall picture aligns with the expectation that sudden-quench work distributions should be close to Gaussian [22] in generic, short-range settings, but makes that statement precise by pinning it to rigorous CLTs for traces of Haar unitary matrices, and by exhibiting how interaction range and anisotropies feed into the covariance through the coefficients  $\{\alpha_m\}$  [10, 12].

It is also worth stressing that, while we often illustrate with finite-range dispersions, none of our Gaussian conclusions hinge on that restriction. Two complementary routes guarantee a Gaussian core: (i) the Szegő regularity condition  $\sum_{r \geq 1} r(a_r^2 + b_r^2) < \infty$ , which covers analytic (and many mildly non-analytic) symbols; and (ii) truncation to  $m(N)$  harmonics with  $m(N) \rightarrow \infty$  but  $m(N) = o(N^{2/3})$ , for which a quantitative multivariate CLT for  $(\Re \text{Tr } U^r, \Im \text{Tr } U^r)_{r \leq m(N)}$  yields the same limiting Gaussian with variance  $\frac{1}{2} \sum_{r \geq 1} r(a_r^2 + b_r^2)$  [19] (and a super-exponential error if  $m \ll \sqrt{N}$ ). We return to this point in Sec. IV.

**Organization.**— In Section II, we present the matrix model and Toeplitz determinant description for finite-range quadratic chains and initial Gaussian and domain wall states. In Section III, we prove the generator identity and pushforward law. In Section IV, we derive the Gaussian core from the well-known central limit theorems in random matrix theory for traces of unitaries, giving the explicit covariance. We then specialise in quadratic fermionic models, including pairing models such as the XY model. We isolate the mechanisms responsible for non-Gaussian tails, such as the presence of many harmonics in the dispersion relation of the fermionic model, the occurrence of Fisher–Hartwig singularities (which are non-analytic jumps or zeros in the symbol of the Toeplitz matrix [21, 23]) and the existence of Fisher zeros (zeros of the Loschmidt amplitude in the complex time plane [11, 12]) near the real axis. This is illustrated using the XY chain (Sec. V). Numerical diagnostics (histograms, quantile-quantile (Q–Q) plots, and variance/kurtosis versus  $N$ ) support the theory (Section VI). The outlook (section VII) suggests further work on open boundary conditions

<sup>1</sup> We illustrate with finite range in formulas for brevity; the Gaussian core does not rely on this and extends to infinite-range symbols under  $\sum_{r \geq 1} r(a_r^2 + b_r^2) < \infty$ , or to truncations with  $m(N) = o(N^{2/3})$ , cf. Sec. IV.

(OBC), Fisher–Hartwig singularities and across-critical quenches, as well as considering multicritical extensions by tuning the parameters  $a_r$ .

## II. SETUP

**Model and conventions.**— We work with spinless fermions on a ring of length  $L$  with periodic boundary conditions (PBC). The lattice operators  $c_j$  and  $c_j^\dagger$  annihilate/create a fermion at site  $j$  and obey the canonical anticommutation relations (CAR)

$$\{c_i, c_j\} = 0, \quad \{c_i^\dagger, c_j^\dagger\} = 0, \quad \{c_i, c_j^\dagger\} = \delta_{ij}. \quad (12)$$

With the discrete Brillouin set  $\mathcal{B} = \{2\pi n/L : n = 0, 1, \dots, L-1\}$  we use

$$c_k := \frac{1}{\sqrt{L}} \sum_{j=1}^L e^{-ikj} c_j, \quad c_j = \frac{1}{\sqrt{L}} \sum_{k \in \mathcal{B}} e^{ikj} c_k, \quad (13)$$

so that  $\{c_k, c_{k'}^\dagger\} = \delta_{k,k'}$  and other anticommutators vanish. We set  $\hbar = 1$  throughout. We consider finite-range, translation-invariant quadratic fermion chains on a ring of length  $L$  with periodic boundary conditions (PBC). In real space,

$$\begin{aligned} H = & \sum_{j=1}^L \sum_{r=1}^m \left( J_r c_{j+r}^\dagger c_j + \overline{J_r} c_j^\dagger c_{j+r} \right) \\ & + \sum_{j=1}^L \sum_{r=1}^m \left( \Delta_r c_{j+r}^\dagger c_j^\dagger + \overline{\Delta_r} c_j c_{j+r} \right) + \mu \sum_{j=1}^L c_j^\dagger c_j. \end{aligned} \quad (14)$$

We call the number-conserving case  $\Delta_r \equiv 0$  *XX-type* (unpaired), and the case  $\Delta_r \neq 0$  *paired/Bogoliubov-de Gennes (BdG)*. For background on the free-fermion/spin-chain correspondence and diagonalization, see [24–26]. For the BdG/Nambu formalism and Gaussian-state technology, see [27–29].

**Momentum-space form.** After a Fourier transform (to  $k = \frac{2\pi}{L}\mathbb{Z}$ ) and, when pairing is present, writing operators in the Nambu basis  $\Psi_k = (c_k, c_{-k}^\dagger)^T$ , the Hamiltonian decouples into  $2 \times 2$  blocks with Pauli matrices  $(\sigma_x, \sigma_y, \sigma_z)$

$$H = \sum_k \Psi_k^\dagger H(k) \Psi_k, \quad H(k) = \xi(k) \sigma_z + \Delta(k) \sigma_y, \quad (15)$$

with single-particle dispersion  $\varepsilon(k) = 2\sqrt{\xi(k)^2 + \Delta(k)^2}$ . For finite range  $m$ ,

$$\xi(k) = 2 \sum_{r=1}^m \Re(J_r) \cos(rk) - \mu, \quad (16)$$

$$\Delta(k) = 2 \sum_{r=1}^m \Re(\Delta_r) \sin(rk). \quad (17)$$

The unpaired case corresponds to  $\Delta \equiv 0$ ; pairing simply activates the sine harmonics through  $\Delta(k)$ .

**Initial states.** We use two standard Gaussian preparations: (i) a translation-invariant Slater/BCS eigenstate of  $H_i$  (typically its ground state); and (ii) a *domain-wall* Slater state occupying a contiguous block  $A \subset \{1, \dots, L\}$ ,

$$|\text{DW}_A\rangle = \prod_{j \in A} c_j^\dagger |0\rangle, \quad (18)$$

$$C_{ij} = \langle \text{DW}_A | c_i^\dagger c_j | \text{DW}_A \rangle = \mathbf{1}_{\{i=j \in A\}}. \quad (19)$$

Under PBC, case (i) yields for the Loschmidt amplitude a (block-)Toeplitz determinant with symbol built from  $e^{-it\varepsilon(k)}$  (and the Bogoliubov angles in the paired case); see the Heine–Szegő framework and its block extensions in [5, 30, 31]. For the domain-wall state, translation symmetry is broken and one obtains Toeplitz *minors* [6] formed from the restricted propagator; see [4, 32, 33]. These reductions are the starting point for our matrix-model/Toeplitz analysis of  $\chi_W(u)$  developed below.

For a sudden quench from  $H_i$  to  $H_f$  with  $|\psi_0\rangle$  an  $H_i$  eigenstate, the work characteristic function equals the Loschmidt amplitude,  $\chi_W(u) = \langle e^{iuW} \rangle = G(-u)$  and  $P(W) = (2\pi)^{-1} \int e^{-iuW} G(u) du$ . For the number-conserving (XX-type) case under PBC and a translation-invariant Slater/BCS initial state,  $G_N(t)$  is a Toeplitz determinant with symbol  $f_t(e^{i\theta}) = e^{-it\varepsilon(\theta)}$ ; for a domain-wall Slater state,  $G_N(t)$  becomes a Toeplitz *minor* built from the restricted propagator (see [4, 32, 33]). For range- $m$  hoppings  $J_r$  the one-body dispersion is  $\varepsilon(\theta) = 2 \sum_{r=1}^m J_r \cos(r\theta)$  and the symbol is  $f_t(\theta) = \exp(-it\varepsilon(\theta)) = \exp(-i \sum_{r=1}^m a_r \cos(r\theta))$  with

$$a_r = 2J_r \quad (\text{PBC, XX normalization}). \quad (20)$$

Consequently the work random variable can be written as the linear statistic (that is, a weighted sum of  $\cos r\theta_j$  and  $\sin r\theta_j$  modes)

$$W = \sum_{r=1}^m a_r \Re \text{Tr} U^r, \quad U \sim \text{Haar on } U(N). \quad (21)$$

With pairing terms, as in the XY chain, the symbol has both  $\cos(r\theta)$  and  $\sin(r\theta)$  contributions and (21) generalizes to  $W = \sum_{r \leq m} (a_r \Re \text{Tr} U^r + b_r \Im \text{Tr} U^r)$ . *Pairing* here means quadratic Bogoliubov-de Gennes terms that do not conserve particle number—i.e., anomalous terms  $c_k c_{-k}$  and  $c_{-k}^\dagger c_k^\dagger$ —equivalently, a nonzero off-diagonal gap  $\Delta(k)$  in the  $2 \times 2$  BdG block. This setting will be studied further in Section V.

**Exact identification of the generator.** Let  $U \sim \text{Haar on } U(N)$  with eigenangles  $\{\theta_j\}_{j=1}^N$ . For real vectors  $(x_1, \dots, x_m)$  and  $(y_1, \dots, y_m)$  define

$$V(\theta) = i \sum_{r=1}^m (x_r \cos r\theta + y_r \sin r\theta), \quad f(\theta) = e^{V(\theta)}. \quad (22)$$

**Lemma 1** (Exact generator identity (Heine–Szegő)). *For any fixed  $m$  and  $N \in \mathbb{N}$ ,*

$$D_N(e^V) = \mathbb{E}_{U(N)} \exp\left(i \sum_{r=1}^m [x_r \Re \text{Tr } U^r + y_r \Im \text{Tr } U^r]\right). \quad (23)$$

*Proof.* Diagonalize  $U = V \text{diag}(e^{i\theta_1}, \dots, e^{i\theta_N}) V^*$ . Heine–Szegő gives  $D_N(e^V) = \mathbb{E} \prod_{j=1}^N e^{V(\theta_j)} = \mathbb{E} \exp\left(\sum_{j=1}^N V(\theta_j)\right)$ . Since  $\sum_j \cos r\theta_j = \Re \text{Tr } U^r$  and  $\sum_j \sin r\theta_j = \Im \text{Tr } U^r$ , we obtain (23).  $\square$

**Corollary 1** (Work/Loschmidt generator). *With  $\varepsilon(\theta) = 2 \sum_{r \leq m} J_r \cos r\theta$  (and optional pairing  $b_r \sin r\theta$ ), the Loschmidt amplitude is  $G_N(t) = D_N(e^{-it\varepsilon})$ . Up to the conventional sign in  $\chi_W(u) = G(-u)$ , the work characteristic function is the generator along the ray  $(x_r, y_r) = (u a_r, u b_r)$  with  $a_r = 2J_r$ :*

$$\chi_W(u) = \mathbb{E} \exp\left(iu \sum_{r \leq m} [a_r \Re \text{Tr } U^r + b_r \Im \text{Tr } U^r]\right). \quad (24)$$

*Thus the Fourier transform of the Toeplitz model for  $G_N$  is exactly the joint moment generator of  $(\Re \text{Tr } U^r, \Im \text{Tr } U^r)_{r \leq m}$  evaluated on a one-dimensional ray. In other words,  $\chi_W(u)$  equals the moment-generating function of the multivariate random vector  $(\Re \text{Tr } U^r, \Im \text{Tr } U^r)_{r \leq m}$  evaluated along the specific line  $(x_r, y_r) = (u a_r, u b_r)$  in its parameter space.”*

The physical couplings  $J_r$  map to mode coefficients via (20). Therefore,

$$\text{Var}(W) = \frac{1}{2} \sum_{r=1}^m r a_r^2 = 2 \sum_{r=1}^m r J_r^2, \quad (25)$$

and, with pairing coefficients  $b_r$ ,  $\text{Var}(W) = \frac{1}{2} \sum_r r (a_r^2 + b_r^2)$ . Different neighbor ranges contribute additively.

### III. FOURIER TRANSFORM OF LOSCHMIDT AMPLITUDE: $P(W)$ AS LINEAR STATISTICS OF CUE EIGENANGLES

We make explicit why Toeplitz determinants with symbol  $e^{iu\varepsilon(\theta)}$  are *characteristic functions* of linear statistics of CUE eigenangles. This explains that the inverse Fourier transform produces the *law* of such a linear statistic (shifted by the initial energy).

*Setup.* Let  $U \sim \text{Haar}$  on  $U(N)$  with eigenangles  $\{\theta_j\}_{j=1}^N$ . Fix a real  $2\pi$ -periodic  $\varepsilon$  with Fourier expansion

$$\varepsilon(\theta) = \varepsilon_0 + \sum_{r \geq 1} (\alpha_r \cos r\theta + \beta_r \sin r\theta), \quad \alpha_r, \beta_r \in \mathbb{R}. \quad (26)$$

Define the (real) linear statistic

$$S_N(U) := \sum_{j=1}^N \varepsilon(\theta_j) = N\varepsilon_0 + \sum_{r \geq 1} (\alpha_r \Re \text{Tr } U^r + \beta_r \Im \text{Tr } U^r). \quad (27)$$

Using Lemma 1, we are now going to state and prove Theorem 1, which establishes that the work distribution  $P(w)$  is the distribution of the random variable  $S_N(U) - E_0$ , i.e. a linear combination of random matrix traces offset by the initial energy.

**Theorem 1** (Work characteristic function and law).

(i) *Characteristic function. Let  $|\psi_0\rangle$  be an eigenstate of  $H_i$  with  $H_i|\psi_0\rangle = E_0|\psi_0\rangle$ .  $|\psi_0\rangle$  is an eigenstate of  $H_i$  with  $H_i|\psi_0\rangle = E_0|\psi_0\rangle$  (so  $E_0$  is the initial energy). For a sudden quench to  $H_f$  whose Loschmidt amplitude admits the Toeplitz representation  $G_N(t) = D_N(e^{-it\varepsilon})$ . This Toeplitz determinant form for  $G_N(t)$  holds for translation-invariant free fermion models with PBC, see [3, 4] and Section V below. One has*

$$\begin{aligned} \chi_W(u) &= \langle \psi_0 | e^{iuH_f} e^{-iuH_i} | \psi_0 \rangle \\ &= e^{-iuE_0} D_N(e^{iu\varepsilon}) \\ &= e^{-iuE_0} \mathbb{E} e^{iu S_N(U)}. \end{aligned} \quad (28)$$

*So, using Lemma 1 (with  $x_r = u a_r, y_r = u b_r$  per Corollary 1), we identified  $D_N(e^{iu\varepsilon}) = E[\exp(iu S_N(U))]$ . Then  $\chi_W(u) = e^{-iuE_0} D_N(e^{iu\varepsilon}) = e^{-iuE_0} E[e^{iu S_N(U)}]$ , proving (i).*

(ii) *Fourier inversion and pushforward law. Let  $P_N$  denote the work law. As a tempered distribution on  $\mathbb{R}$ ,*

$$P_N(w) = \frac{1}{2\pi} \int_{-\infty}^{\infty} e^{-iuw} \chi_W(u) du. \quad (29)$$

*Equivalently, for every Schwartz test function  $\varphi \in \mathcal{S}(\mathbb{R})$ ,*

$$\int_{\mathbb{R}} \varphi(w) P_N(dw) = \mathbb{E}[\varphi(S_N(U) - E_0)]. \quad (30)$$

*In particular, in Dirac notation,  $P_N = \mathbb{E}[\delta(\cdot - (S_N(U) - E_0))]$  (distributionally). This means that  $P_N(w)$  is the probability law of  $S_N(U) - E_0$  when  $U$  is Haar-random (this is the meaning of (30), interpreting the result as a (tempered) distribution).*

*Sketch of proof.* Let  $\widehat{\varphi}(u) := \int_{\mathbb{R}} e^{-iuw} \varphi(w) dw$ . By part (i),  $\chi_W(u) = e^{-iuE_0} \mathbb{E}[e^{iu S_N(U)}]$ . Since  $\widehat{\varphi} \in \mathcal{S}(\mathbb{R}) \subset L^1(\mathbb{R})$ , Tonelli/Fubini applies and

$$\begin{aligned} \int \varphi(w) P_N(dw) &= \frac{1}{2\pi} \int \widehat{\varphi}(u) \chi_W(u) du \\ &= \frac{1}{2\pi} \int \widehat{\varphi}(u) e^{-iuE_0} \mathbb{E}[e^{iu S_N(U)}] du \\ &= \mathbb{E}\left[\frac{1}{2\pi} \int \widehat{\varphi}(u) e^{iu(S_N(U) - E_0)} du\right] \\ &= \mathbb{E}[\varphi(S_N(U) - E_0)], \end{aligned} \quad (31)$$

*which proves (30).*



*Remarks.* (1) *What is and is not Fourier-transformed.* By Lemma 1 and Theorem 1(i),  $D_N(e^{iu\varepsilon})$  is (up to the trivial phase  $e^{-iuE_0}$ ) the *characteristic function* of the real linear statistic  $S_N(U)$ , see Eq. (20); hence it is positive-definite and satisfies  $\chi_W(0) = 1$ . The inverse Fourier transform acts on this characteristic function in the  $u$ -variable and, in the tempered sense, yields the pushforward law in Eq. (29) (equivalently Eq. (30)). In particular,

$$P_N = \mathbb{E}[\delta(\cdot - (S_N(U) - E_0))] \quad (\text{as distributions}).$$

Crucially, nothing is Fourier-transformed pointwise in the angle  $\theta$ : the symbol  $e^{iu\varepsilon(\theta)}$  enters through the Toeplitz/matrix-model identity that produces the characteristic function; the Fourier inversion is only in  $u$ .

(2) Note that each trace  $\text{Tr } U^r$  is complex, so writing  $S_N$  in terms of  $\Re \text{Tr } U^r$  and  $\Im \text{Tr } U^r$  emphasizes that each mode contributes two independent Gaussian degrees of freedom. In other words, each trace is like a 2D Gaussian (pair of quadratures), ensuring  $S_N$  is a real linear combination of those 2D components

(3) *Centering and variance.* Since  $\mathbb{E}[\text{Tr } U^r] = 0$ , we have  $\mathbb{E}[S_N] = N\varepsilon_0$  and

$$\text{Var}(S_N - N\varepsilon_0) = \frac{1}{2} \sum_{r \geq 1} r(\alpha_r^2 + \beta_r^2) \quad (\text{exact for } N \geq \max r), \quad (32)$$

using  $\mathbb{E}|\text{Tr } U^r|^2 = \min\{r, N\}$  and orthogonality across different  $r$  (see next Section for more on orthogonality). Notice that the real and imaginary parts of each  $T_r$  are independent Gaussians with variance  $r/2$  and this is why the variance (32) is a simple sum of contributions.

**Corollary 2** (Gaussian core with a growing number of modes). *Let  $U \sim \text{Haar}$  on  $U(N)$  and set*

$$W_N = \sum_{r \geq 1} (a_r \Re \text{Tr } U^r + b_r \Im \text{Tr } U^r).$$

*Assume the Szegő regularity  $\sum_{r \geq 1} r(a_r^2 + b_r^2) < \infty$ . For any sequence  $m(N) \rightarrow \infty$  with  $m(N) = o(N^{2/3})$ , write*

$$W_N = W_N^{(\leq m)} + R_N^{(> m)}, \quad (33)$$

*with the truncation*

$$W_N^{(\leq m)} := \sum_{r=1}^{m(N)} (a_r X_r + b_r Y_r), \quad (34)$$

$$\text{with } X_r := \Re \text{Tr } U^r, \quad Y_r := \Im \text{Tr } U^r.$$

*Then, as  $N \rightarrow \infty$ ,*

$$W_N \Rightarrow \mathcal{N}\left(0, \frac{1}{2} \sum_{r \geq 1} r(a_r^2 + b_r^2)\right). \quad (35)$$

*Moreover, for each compact  $K \subset \mathbb{R}$ ,*

$$\sup_{u \in K} |\chi_{W_N}(u) - e^{-u^2 \sigma^2 / 2}| \rightarrow 0. \quad (36)$$

$$\sigma^2 = \frac{1}{2} \sum_{r \geq 1} r(a_r^2 + b_r^2).$$

*In addition, if  $m(N) \ll \sqrt{N}$  then the total-variation error for  $W_N^{(\leq m)}$  is super-exponentially small in  $N/m(N)$  [19]. Sketch. By the multivariate CLT for traces [19], the  $2m(N)$ -vector  $(X_1, Y_1, \dots, X_{m(N)}, Y_{m(N)})$ , scaled by  $\sqrt{r/2}$  on each coordinate, converges (in total variation) to a centered Gaussian in  $\mathbb{R}^{2m(N)}$  whenever  $m(N) = o(N^{2/3})$ , with a super-exponential rate if  $m \ll \sqrt{N}$ . Hence  $W_N^{(\leq m)}$  is asymptotically  $\mathcal{N}(0, \frac{1}{2} \sum_{r \leq m(N)} r(a_r^2 + b_r^2))$ . The tail has vanishing variance,  $\text{Var } R_N^{(> m)} = \frac{1}{2} \sum_{r > m(N)} r(a_r^2 + b_r^2) \rightarrow 0$ , so (36) follows by Slutsky's lemma.*

#### IV. GAUSSIAN CORE: WHY TRACES OF POWERS ARE ASYMPTOTICALLY INDEPENDENT GAUSSIANS

Let  $U \sim \text{Haar}$  on  $U(N)$  and write  $T_r := \text{Tr } U^r = \sum_{j=1}^N e^{ir\theta_j}$ . Already at finite  $N$  one has [16, 17]

$$\mathbb{E}|T_r|^2 = \min\{r, N\}, \quad \mathbb{E}T_r = 0, \quad \mathbb{E}T_r T_s = 0 \quad (r \neq s), \quad (37)$$

fixing the *random-matrix normalization*: the natural scale is  $\sqrt{r}$  (rather than  $\sqrt{N}$ ). For any fixed  $m$ , “we have convergence in distribution to i.i.d. complex Gaussians, namely

$$\left(\frac{T_1}{\sqrt{1}}, \frac{T_2}{\sqrt{2}}, \dots, \frac{T_m}{\sqrt{m}}\right) \xrightarrow[N \rightarrow \infty]{d} (Z_1, \dots, Z_m), \quad (38)$$

with  $Z_r$  i.i.d. standard complex Gaussians. Equivalently,

$$\mathbb{E}[T_r] = 0, \quad \mathbb{E}[T_r \overline{T_s}] = \delta_{rs} r, \quad \mathbb{E}[T_r T_s] = 0. \quad (39)$$

So, different trace powers become independent Gaussians in the large- $N$  limit and it is the orthogonality  $\mathbb{E}[T_r T_s] = 0$  for  $r \neq s$  the reason the joint distribution factorizes. There are two complementary derivations which are physically illuminating.

(i) *Toeplitz/cumulants (strong Szegő).* Heine–Szegő identifies  $D_N(e^{iu\varepsilon})$  with the characteristic function of  $S_N = \sum_j \varepsilon(\theta_j) = \sum_r (\alpha_r \Re T_r + \beta_r \Im T_r) + N\varepsilon_0$ . The strong Szegő limit theorem expands  $\log D_N$  into cumulants and shows that as  $N \rightarrow \infty$  [18]

$$\log D_N(e^{iu\varepsilon}) = iu N\varepsilon_0 - \frac{u^2}{4} \sum_{r \geq 1} r(\alpha_r^2 + \beta_r^2) + o(1), \quad (40)$$

so  $\kappa_1(S_N) = N\varepsilon_0$ ,  $\kappa_2(S_N) = \frac{1}{2} \sum_r r(\alpha_r^2 + \beta_r^2)$ , and  $\kappa_p(S_N) \rightarrow 0$  for  $p \geq 3$ . Recall that  $o(1)$  denotes a term that vanishes as  $N \rightarrow \infty$ .

(ii) *Direct multivariate CLT for traces.* K. Johansson [18] established the CLT for linear statistics and

Johansson and Lambert [19] gave quantitative multivariate bounds (TV metric) and growth windows for  $m(N)$ . More precisely, they have proven a quantitative multivariate central limit theorem for  $(T_1, \dots, T_m)$  (after  $\sqrt{r}$  rescaling) including explicit error bounds, even allowing  $m$  to grow moderately with  $N$ . More precisely, the multivariate CLT remains valid uniformly for  $m = o(N^{2/3})$  and when  $m(N) = o(\sqrt{N})$  the total-variation error is super-exponentially small in  $N/m$  [19]. This is convenient for controlling  $\chi_W(u)$  uniformly on compact  $u$ -intervals.

Under any of these  $m(N)$  growth values, for any fixed  $m$  and coefficients  $\{a_r, b_r\}_{r \leq m}$ ,

$$W = \sum_{r=1}^m (a_r \Re T_r + b_r \Im T_r) \implies \mathcal{N}\left(0, \frac{1}{2} \sum_{r=1}^m r(a_r^2 + b_r^2)\right). \quad (41)$$

This is our *Gaussian core* for  $P(W)$ , verified below numerically. The Gaussian core is visible in the straight quantile-quantile plots, e.g. Fig. 1(b,e) and Fig. 2(b,e).

*Finite- $N$  corrections and growth of  $m$ .* At fixed  $m$ , the leading non-Gaussian features are governed by the third and fourth cumulants. When  $m$  grows with  $N$ , the multivariate bounds of Johansson–Lambert quantify how fast  $m$  may increase while  $(T_1, \dots, T_m)$  stays close (in total variation) to its Gaussian limit. Finite- $N$  deviations appear only in the extremes (detrended Q-Q): see Fig. 1(c,f) and Fig. 2(c,f). The surrogate and exact Haar data are indistinguishable in the bulk (compare Fig. 3, rows 2–3).

Different powers  $r \neq s$  are uncorrelated (indeed asymptotically independent), which justifies the variance additivity in (32) and later formulas.

#### A. Products of traces: selection rules, Wick limits, and large- $N$ structure

Many observables with couplings to 1st, 2nd,  $\dots$ ,  $m$ -th neighbors lead to correlators of products of traces such as  $\mathbb{E}[\prod_{r \leq m} T_r^{\alpha_r} \overline{T}_r^{\beta_r}]$ . Two structural facts guide computations.

*Selection rule (exact for all  $N$ ).* Invariance under the global phase  $U \mapsto e^{i\phi} U$  implies

$$\mathbb{E}\left[\prod_{a=1}^p T_{k_a} \prod_{b=1}^q \overline{T}_{\ell_b}\right] = 0 \quad \text{unless} \quad \sum_{a=1}^p k_a = \sum_{b=1}^q \ell_b. \quad (42)$$

So, this invariance is why any moment with an unmatched number of  $T$  factors vanishes. In particular  $\mathbb{E}[T_1 T_2 \dots T_m] = 0$  for all  $m \geq 1$ .

*Wick factorization (asymptotic).* Since (38) holds with independent complex Gaussian limits,

$$\mathbb{E}\left[\prod_{r=1}^m T_r^{\alpha_r} \overline{T}_r^{\beta_r}\right] = \prod_{r=1}^m (\delta_{\alpha_r, \beta_r} \alpha_r! r^{\alpha_r}) + o(1). \quad (43)$$

This means that mixed moment factorizes into second moments (pairings) plus  $o(1)$ . Thus, at leading order, only pairings  $T_r$  with  $\overline{T}_r$  survive; cross-pairings between different powers are subleading. Two basic consequences are, with  $r, s$  fixed,  $N \rightarrow \infty$

$$\mathbb{E}|T_r|^{2q} = q! r^q + o(1), \quad \mathbb{E}[T_r \overline{T}_s] = \delta_{rs} r. \quad (44)$$

The lack of cross-covariance and the  $\sqrt{r/2}$  scaling are borne out by the scatter panels with 95% ellipses; see Fig. 5(a,b) and the standardized versions in Fig. 5(c,d).

### V. QUADRATIC FERMIONIC CHAINS, GAUSSIAN CORE, AND NON-GAUSSIAN TAILS

We henceforth absorb factors of 2 into the coefficients and refer to the Fourier components as  $a_r$  (from  $\cos r\theta$  terms of  $\epsilon$ ) and  $b_r$  (from  $\sin r\theta$  terms), for consistency with earlier sections. In particular, the examples below use  $a_r$  and  $b_r$ , as given below in (48).

#### A. Starting point: a general quadratic chain (with pairing)

Consider a translation-invariant quadratic fermionic Hamiltonian (with possible pairing) that, after Fourier and Nambu (BdG) lifting, decouples as

$$H = \sum_{k \in \mathcal{B}} \Psi_k^\dagger \mathcal{H}(k) \Psi_k, \quad \mathcal{H}(k) = \xi(k) \sigma_z + \Delta(k) \sigma_y, \quad (45)$$

with dispersion  $\varepsilon(k) = 2\sqrt{\xi(k)^2 + \Delta(k)^2}$  and a Brillouin set  $\mathcal{B}$ . For a sudden quench from  $H_i$  to  $H_f$ , the work characteristic function

$$\chi_W(u) = \langle e^{iuH_f} e^{-iuH_i} \rangle_{\psi_0} = e^{-iuE_0} \langle \psi_0 | e^{iuH_f} | \psi_0 \rangle \quad (46)$$

is representation-invariant; it factorizes over  $k$  and admits a compact determinant/Pfaffian form. Under PBC and translation invariance,  $\log \chi_W(u)$  is a Riemann sum over  $k$  that, upon Fourier expansion in  $\theta$ , reduces to the Toeplitz model used above:

$$\chi_W(u) = D_N \left( e^{i \sum_{r \geq 1} [x_r \cos(r\theta) + y_r \sin(r\theta)]} \right), \quad (47)$$

with coefficients  $(x_r, y_r)$  determined by the Fourier content of  $\varepsilon$  together with the Bogoliubov angles that encode the initial BCS vacuum. Consequently the work variable is the linear statistic

$$W = \sum_{r \geq 1} (a_r \Re \text{Tr } U^r + b_r \Im \text{Tr } U^r), \quad (48)$$

where  $a_r \propto \hat{\varepsilon}_r^{(\cos)}$  and  $b_r \propto \hat{\varepsilon}_r^{(\sin)}$  (pairing produces the sine-harmonics). We stress that in (47), the coefficients  $x_r$  and  $y_r$  are directly related to the Fourier expansion of the single-particle energy  $\epsilon(k)$ . Writing

$\epsilon(\theta) = \epsilon_0 + \sum r \geq 1 [\epsilon_r^{(c)} \cos(r\theta) + \epsilon_r^{(s)} \sin(r\theta)]$ , and noting that pairing (nonzero  $\Delta(k)$ ) contributes sine terms via the Bogoliubov rotation, one finds  $x_r = u, \epsilon_r^{(c)}$  and  $y_r = u, \epsilon_r^{(s)}$ . Equivalently,  $a_r = \epsilon_r^{(c)}$  and  $b_r = \epsilon_r^{(s)}$  in the notation of (48) (up to the factor of 2 coming from the Jordan-Wigner convention, cf. Corollary 1).

The fact that the initial state is a *Bogoliubov* (BCS) vacuum rather than the Jordan–Wigner vacuum merely changes the values of  $\{a_r, b_r\}$ ; the identities  $\chi_W(u) = G(-u)$  and the Toeplitz representation are unaffected.

### B. When the Gaussian core is guaranteed

Let  $V(\theta) = iu\varepsilon(\theta) = iu(\varepsilon_0 + \sum_{r \geq 1} (\alpha_r \cos r\theta + \beta_r \sin r\theta))$ . The strong Szegő condition

$$\sum_{r \geq 1} r |\widehat{V}_r|^2 = u^2 \sum_{r \geq 1} r(\alpha_r^2 + \beta_r^2) < \infty \quad (V \in H^{1/2}) \quad (49)$$

is satisfied whenever  $\varepsilon$  has Fourier modes decaying a bit faster than  $1/r$ . Under (49): (i) the cumulant expansion gives  $\kappa_1(S_N) = N\varepsilon_0$ ,  $\kappa_2(S_N) = \frac{1}{2} \sum_{r \geq 1} r(\alpha_r^2 + \beta_r^2)$  and  $\kappa_p(S_N) \rightarrow 0$  for  $p \geq 3$ ; (ii) the multivariate CLT for  $(T_1, \dots, T_m)$  after  $\sqrt{r}$  rescaling holds for fixed  $m$ , with quantitative extensions when  $m = m(N)$  grows slowly. Therefore, for  $W = \sum_{r \leq m} (a_r \Re T_r + b_r \Im T_r)$  one has

$$W \Rightarrow \mathcal{N}\left(0, \frac{1}{2} \sum_{r \leq m} r(a_r^2 + b_r^2)\right) \quad (N \rightarrow \infty). \quad (50)$$

It is worth stressing that the strong Szegő condition (49) is what guarantees the Gaussian core rigorously:  $W$  converges in distribution to  $\mathcal{N}(0, \frac{1}{2} \sum_{r \leq m} r(a_r^2 + b_r^2))$ . Two useful corollaries: (1) if  $\varepsilon$  is real-analytic (gapped models, generic BdG), then  $(a_r, b_r)$  decay exponentially and the Gaussian core is extremely sharp; (2) even with mild cusps (e.g., linear dispersion near a gap closing), the sum in (49) typically converges, so the core remains Gaussian while finite- $N$  corrections increase. The exponential vs. power-law Fourier decay manifests exactly as expected: the exponential case shows a virtually perfect Q–Q line, while the power-law case exhibits mild tail curvature (Fig. 2(e) vs. Fig. 2(b,c)).

### C. Where non-Gaussian tails come from

In several physically relevant mappings, such as for the case of open boundary conditions presented in [4] the symbol picks up genuine Fisher–Hartwig (FH) singularities such as algebraic endpoints and/or jump phases, unlike the PBC case studied here, where  $\epsilon(\theta)$  is smooth unless crossing a critical point. A canonical FH symbol has the form, with  $\alpha_j > -1/2$  [5]

$$f_{\text{FH}}(\theta) = e^{V(\theta)} \prod_{j=1}^J |2 - 2 \cos(\theta - \theta_j)|^{\alpha_j} e^{i\beta_j(\theta - \theta_j - \pi)}. \quad (51)$$

For such symbols, the Toeplitz asymptotics depart from the pure strong Szegő quadratic law:  $D_N(f_{\text{FH}})$  exhibits explicit  $N$ -dependent power laws, oscillatory factors, and constant terms determined by the FH data  $\{\alpha_j, \beta_j, \theta_j\}$ .

Under PBC, Loschmidt symbols naturally enter the Fisher–Hartwig (FH) class whenever the quench creates discontinuities at Fermi points or algebraic endpoints. For a *flux (twist) quench* without pairing, one has a scalar Toeplitz symbol  $f_t(e^{i\theta}) = \exp(it\varepsilon(\theta))g(\theta)$  in which  $g$  carries *jump* FH singularities at the (pre/post) Fermi points  $\{\theta_j\}$  with exponents  $\beta_j \neq 0$ ; expanding  $\log f_t(\theta) = \sum_{m \neq 0} c_m e^{im\theta}$  gives  $c_m^{(j)} = \frac{i\beta_j}{m} e^{-im\theta_j}$  and, by Heine–Szegő plus the covariance  $\mathbb{E}|\text{Tr } U^m|^2 = m$  [16, 18], the linear statistic variance scales as

$$\text{Var}(\log G_N) = \sum_{m \leq N} m |c_m|^2 = \left( \sum_j \beta_j^2 \right) \log N + O(1),$$

i.e. FH enhances fluctuations to a  $\sqrt{\log N}$  scale while the *Gaussian core* from the smooth part (Szegő) remains.

For quenches with pairing (XY or Ising case, to be further discussed below), the object is a *block Toeplitz* determinant with  $2 \times 2$  symbol  $\Phi(k, t) = (\mathbb{I} - \mathcal{C}_0(k)) + \mathcal{C}_0(k)e^{-i\mathcal{H}_1(k)t}$ ; quenches across criticality generate *root* FH exponents at  $k = 0, \pi$  ( $\alpha = \pm \frac{1}{2}$ ) and possibly jumps ( $\beta \neq 0$ ), producing deterministic power-law/oscillatory factors on top of the same CLT-driven Gaussian core for the finite Fourier harmonics of  $\log \det \Phi$ . Thus, in PBC as in the OBC case that will be discussed elsewhere, the trace-statistics mechanism gives the Gaussian center, while the FH data dictate the normalization and non-Gaussian tails.

Non-Gaussian features arise when at least one hypothesis behind Szegő/CLT degrades. In particular:

(A) *Too many modes / slow decay.* If the effective number of harmonics  $m$  grows with  $N$  and  $(a_r, b_r)$  decay slowly, higher cumulants need not vanish. A sufficient condition for a stable Gaussian core is  $\sum_{r \geq 1} r(a_r^2 + b_r^2) < \infty$  together with admissible growth  $m(N)$  (cf. Johansson–Lambert). At the borderline  $a_r, b_r \sim r^{-1}$  the variance diverges logarithmically and the correct scaling changes (non-Gaussian-looking histograms at fixed normalization). That is, a very large number of Fourier modes or a dispersion whose Fourier coefficients  $a_r, b_r$  decay too slowly (borderline  $1/r$  behavior or weaker) can invalidate the central limit approximation. See the tail curvature in detrended Q–Q, Fig. 2(c).

(B) *Fisher–Hartwig singularities.* In variants where the symbol develops genuine FH factors, which are nonanalytic features in the symbol such as jump discontinuities or zeros [21],  $\log D_N$  contains non-quadratic terms (power-laws/oscillations), and persistent non-Gaussian edges appear. This includes certain OBC reductions and

matrix-model weights related to Painlevé V [4] (to be discussed elsewhere).

(C) *Critical quenches / DQPTs.* Crossing a quantum critical manifold brings Fisher zeros of  $G(t)$  close to the real axis. Indeed, if the quench crosses a phase transition, the Loschmidt amplitude develops Fisher zeros arbitrarily close to the real axis, which translates into  $\chi_W(u)$  acquiring singularities for real  $u$  (non-analytic behavior in time). This will thicken the tails of  $P(W)$ . Persistent edge features (cf. discussion here; qualitative signature matches the residuals in Fig. 1(c,f)).

(D) *Finite- $N$  mesoscopic windows.* For moderate  $N$  or weight on medium/large  $r$ , the third/fourth cumulants—which are  $o(1)$  asymptotically—are visible. Edgeworth corrections from the cumulant method would capture these tails. Notice how small residual deviations are confined to extremes, Fig. 1(c,f).

### 1. The XY chain: square-root dispersion and tails

a. *Model and diagonalization.* After the Jordan–Wigner map, the translation-invariant XY chain in a transverse field is a quadratic (BdG) fermion system [24–26] with

$$\mathcal{H}(k) = \mathbf{d}(k) \cdot \boldsymbol{\sigma}, \quad (52)$$

$$\mathbf{d}(k) = (\gamma \sin k, 0, h - \cos k), \quad (53)$$

$$\varepsilon(k) = 2|\mathbf{d}(k)| = 2\sqrt{(h - \cos k)^2 + (\gamma \sin k)^2}. \quad (54)$$

The *Bogoliubov angle* is

$$\tan(2\theta_k) = \frac{\gamma \sin k}{h - \cos k}, \quad (55)$$

so that a rotation by  $2\theta_k$  in Nambu space diagonalizes  $\mathcal{H}(k)$ .

b. *Loschmidt amplitude and work characteristic function.* For a sudden quench  $(\gamma_i, h_i) \rightarrow (\gamma_f, h_f)$  from the ground state of  $H_i$  (a BCS vacuum), the Loschmidt amplitude and TPM work characteristic function are

$$G(t) := \langle \psi_0 | e^{-iH_f t} | \psi_0 \rangle, \quad \chi_W(u) = e^{-iuE_0} G(-u), \quad (56)$$

with  $H_i |\psi_0\rangle = E_0 |\psi_0\rangle$  [10]. The overlap factorizes over  $(k, -k)$  and admits the standard product form [11]

$$G(t) = \prod_{k>0} \left[ \cos(\varepsilon_f(k)t) - i \sin(\varepsilon_f(k)t) \cos(2\Delta\theta_k) \right], \quad (57)$$

where  $\Delta\theta_k := \theta_k(\gamma_f, h_f) - \theta_k(\gamma_i, h_i)$ .

c. *From block Toeplitz to a scalar symbol.* Equivalently, using the Klich reduction for Gaussian states [29] (and the HFB/Pfaffian viewpoint [27, 28]),

$$\Phi(k, t) = (\mathbb{I} - \mathcal{C}_0(k)) + \mathcal{C}_0(k) e^{-i\mathcal{H}_f(k)t}, \quad (58)$$

with  $\mathcal{C}_0(k) = \frac{1}{2}(\mathbb{I} - \hat{\mathbf{d}}_i(k) \cdot \boldsymbol{\sigma})$ .

For translation-invariant chains this is a *block Toeplitz* operator in real space; see e.g. the block-Toeplitz structure for XY correlation-matrix functionals in [31] and strong Szegő-type expansions for matrix symbols in [30]. A short  $2 \times 2$  calculus gives

$$\det \Phi(k, t) = \left[ \cos(\varepsilon_f(k)t) - i \sin(\varepsilon_f(k)t) \cos(2\Delta\theta_k) \right]^2. \quad (59)$$

Thus the *scalar* symbol

$$f_t(e^{ik}) = \cos(\varepsilon_f(k)t) - i \sin(\varepsilon_f(k)t) \cos(2\Delta\theta_k) \quad (60)$$

controls  $G(t)$  via  $G(t) = \sqrt{\det T_N(\Phi)} = D_N(f_t)^{1/2}$  and (57).

d. *Small- $u$  reduction to traces.* Setting  $u = t$  in  $\chi_W(u) = e^{-iuE_0} G(-u)$  and expanding for small  $u$ ,

$$f_u(e^{ik}) = 1 - iu\tilde{\varepsilon}(k) - \frac{1}{2}u^2\varepsilon_f(k)^2 + O(u^3), \quad (61)$$

$$\tilde{\varepsilon}(k) := \varepsilon_f(k) \cos(2\Delta\theta_k), \quad (62)$$

$$\log f_u(e^{ik}) = -iu\tilde{\varepsilon}(k) + O(u^2). \quad (63)$$

With the Fourier series

$$\tilde{\varepsilon}(k) = \sum_{m \in \mathbb{Z}} \tilde{\alpha}_m e^{imk}, \quad \tilde{\alpha}_m = \frac{1}{2\pi} \int_{-\pi}^{\pi} \tilde{\varepsilon}(k) e^{-imk} dk, \quad (64)$$

Heine–Szegő gives the linear-statistics form

$$\log \chi_W(u) = iu \sum_{m \geq 1} \left( \tilde{\alpha}_m \operatorname{Tr} U^m + \overline{\tilde{\alpha}_m} \operatorname{Tr} U^{-m} \right) + O(u^2), \quad (65)$$

so the selection rule and Wick factorization of Sec. V apply verbatim with  $\varepsilon(k) \mapsto \tilde{\varepsilon}(k)$ . In particular,

$$\sigma^2 = 2 \sum_{m \geq 1} m |\tilde{\alpha}_m|^2. \quad (66)$$

e. *When non-Gaussian tails appear.* If the quench does *not* cross a critical line, then  $k \mapsto f_t(e^{ik})$  is smooth for fixed  $t$ ;  $\tilde{\varepsilon}(k)$  is analytic and the Fourier coefficients  $\tilde{\alpha}_m$  decay exponentially, so the central  $P(w)$  is Gaussian with  $O(1)$  width. If the quench *does* cross a critical line,  $\Delta\theta_k$  acquires an endpoint jump at  $k = 0$  or  $\pi$ ,  $f_t$  becomes piecewise smooth (FH type), and Toeplitz FH asymptotics yield deterministic power-law/oscillatory corrections [23] (visible non-Gaussian tails).

f. *XX limit* For  $\gamma_i = \gamma_f = 0$  one has  $\theta_k \equiv 0$ , hence  $\Delta\theta_k = 0$  and (57) collapses to

$$G(t) = \prod_{k>0} e^{-i\varepsilon_f(k)t}, \quad (67)$$

the translation-invariant, number-conserving XX limit (cf. [24, 25]). This should not be confused with the



*domain-wall XX* protocol analyzed earlier, where  $G_N(t) = D_N(e^{-it\varepsilon})$  is a Toeplitz determinant built from the restricted propagator on a spatial block. Here  $\varepsilon_f(k) = 2|h_f - \cos k|$  is the BdG (positive) branch. If one prefers the Jordan–Wigner convention  $\xi_f(k) = 2(\cos k - h_f)$ , the same reduction is obtained by keeping the piecewise sign in  $\cos(2\Delta\theta_k)$ , which amounts to writing  $e^{-i|\xi_f|t}$  together with jump phases at the Fermi points (FH language). This change of convention does not affect the Gaussian-core variance nor our diagnostics.

## 2. Quick summary of Gaussianity and tail behavior

- *Gapped BdG (analytic  $\varepsilon$ ):* sharp Gaussian core; pairing just introduces  $b_r$  in the variance  $\frac{1}{2} \sum_r r(a_r^2 + b_r^2)$ .
- *Critical (no FH):* core Gaussian; tails show visible but shrinking non-Gaussian corrections.
- *FH/jumps/zeros or borderline decay:* persistent non-Gaussian structures (edges/oscillations); the correct asymptotics are beyond strong Szegő.
- *Large  $m$  or slow decay of  $(a_r, b_r)$ :* the fixed-normalization histogram looks non-Gaussian; after the right rescaling a Gaussian limit often returns.

## VI. NUMERICAL DIAGNOSTICS

We assess Gaussianity and the CLT predictions with four complementary diagnostics: (i) histogram with Gaussian overlay; (ii) normal quantile-quantile plots (Q–Q plots; defined below) (and, when informative, detrended Q–Q); (iii) scatter plots of trace components with theory ellipses, including standardized versions; and (iv) variance and excess kurtosis versus  $N$  with error bars. The full set of panels is shown after the references.

*Notation and basic definitions.* Throughout this section,  $N$  denotes the matrix dimension of  $U(N)$  in the unitary matrix model;  $m$  is the number of active Fourier harmonics in the dispersion (equivalently, the neighbor range retained in the chain); and  $n$  is the number of Monte–Carlo realizations used per panel (sample size behind each histogram or Q–Q plot). A *Q–Q (quantile–quantile) plot* compares the empirical quantiles of the (centered) work variable on the vertical axis to the corresponding theoretical normal quantiles on the horizontal axis; alignment with the line  $y = x$  indicates a Gaussian core, while systematic curvature near the extremes reveals tail deviations. Histograms use the Freedman–Diaconis bin width [34]

$$h = \frac{2 \text{IQR}}{n^{1/3}}, \quad \text{IQR} := Q_{0.75} - Q_{0.25},$$

where IQR is the *interquartile range* (the difference between the 75th and 25th percentiles).

*Sampling and rendering choices.* To display the Gaussian core with low sampling noise, most panels are generated with a surrogate.

We use a Gaussian surrogate that preserves the exact first-/second-moment structure (Sec. IV). To generate surrogate data, we replace the Haar matrix  $U$  by independent complex Gaussian variables:  $\text{Tr } U^r$  is sampled from  $\mathcal{CN}(0, r)$  (a complex normal with mean 0 and variance  $r$ ) for each  $r$ , with different  $r$  samples taken independent. This preserves the exact first- and second-moment structure but assumes asymptotic independence outright. This means that we draw:

$$\text{Tr } U^r \stackrel{d}{\approx} \mathcal{CN}(0, r), \quad (68)$$

independently over the finite set of harmonics and form  $W = 2 \Re \sum_r \alpha_r \text{Tr } U^r$  (Section IV). This reproduces the central limit covariance exactly for fixed  $r$  and large  $N$ , at a fraction of the cost of explicit Haar draws. As a cross-check, we include “Haar vs surrogate” comparisons at  $N = 80$ ,  $n = 300$ , showing near-identical bulk behavior. See Fig. 3 for a Haar vs surrogate comparison. Histograms use the Freedman–Diaconis bin width  $h = 2 \text{IQR}/n^{1/3}$  [34] and overlay the fitted Gaussian  $\mathcal{N}(0, \hat{\sigma}^2)$ . Q–Q plots use the classic “points +  $y = x$ ” style; we also provide *detrended* Q–Q (residuals vs theoretical quantiles), which makes small tail deviations easier to see.

*What the panels show and how to read them.*

1. **Histogram/Q–Q pairs.** High- $n$  panels (histogram with Gaussian overlay; Q–Q with  $y = x$  line) display the Gaussian core and isolate any tail curvature.
2. **Scatter plots.** Clouds of  $(\Re \text{Tr } U^r, \Re \text{Tr } U^s)$  include the *theory 95% ellipse*; standardized versions divide each axis by  $\sqrt{m/2}$  so the contour is a circle, making different  $(r, s)$  pairs comparable.
3. **Variance vs  $N$ .** With fixed harmonics, the CLT variance  $\text{Var}(W) = \frac{1}{2} \sum_r r(a_r^2 + b_r^2)$  is  $N$ -independent; the plot plateaus at this constant (dashed line) with SE bars  $\hat{\sigma}^2 \sqrt{2/(n-1)}$ .
4. **Excess kurtosis vs  $N$ .** The trend toward 0 (with error bars  $\sqrt{24/n}$ ) matches the CLT/Wick picture; residual scatter reflects the estimator’s finite- $n$  noise and small negative bias  $\approx 6/(n+1)$ .

*Compact diagnostics that tie figures to theory.* For a given choice of weights, define

$$S_m = \sum_{r \leq m} r(a_r^2 + b_r^2), \quad T_m = \sum_{r \leq m} r^{3/2}(|a_r|^3 + |b_r|^3).$$

Then  $\text{Var}(W) = \frac{1}{2} S_m$  (prediction for the dashed line in Fig. 4a), while the dimensionless skewness proxy  $T_m/S_m^{3/2}$  tracks the relative size of the cubic cumulant: it is small (and shrinks with  $m$ ) when the Fourier weights decay fast

(analytic symbols, within-phase quenches), and it grows in borderline/FH regimes. This explains why the Q–Q bulk is straight and why any curvature, when present, is confined to the extremes. More precisely, the ratio  $T_m/S_m^{3/2}$  tracks the relative size of cubic cumulants: it  $\rightarrow 0$  under fast decay (Gaussian-looking tails) and grows in borderline regimes. We define  $T_m$  as the weighted  $L^3$ -norm of the mode coefficients (with a factor  $r^{3/2}$  for convenience), and  $S_m$  as the weighted  $L^2$ -norm. The ratio  $T_m/S_m^{3/2}$  is dimensionless and serves as a proxy for the normalized third cumulant (skewness).

If all weight is on a single mode, this ratio would correspond exactly to the skewness of that mode’s distribution. When the ratio is small, it indicates the distribution is close to Gaussian (since higher cumulants are negligible). Figure 4(b) shows how the kurtosis trends to the Gaussian value as  $N$  increases, confirming our CLT-based prediction that  $P(W)$  becomes Gaussian in the large- $N$  limit.

*Summary.* Across the histogram/Q–Q pairs (Figures 1, 2 and 3), and variance/kurtosis trends (Figure 4) and scatter panels (Figure 5) the data agree with the random-matrix CLT for traces: a *Gaussian bulk* with the variance set by the quadratic form  $\sum_r r(a_r^2 + b_r^2)$  and *asymptotic independence* across different powers. Non-Gaussian features, when visible, appear where Szegő hypotheses are weakened (many harmonics, slow decay) or in settings with genuine FH structure (jumps/zeros/edge singularities), in line with the discussion in Sec. V.

## VII. CONCLUSIONS AND OUTLOOK

We mapped the work distribution in a sudden quench onto a random matrix problem (the traces of Haar unitaries). The multivariate central limit theorem then predicts a Gaussian core to the distribution for a large system size,  $N$ , with a variance fully determined by the quench parameters (11). More precisely, this is determined by the Fourier components of the post-quench dispersion. The coefficients,  $\alpha_m$ , come from expanding the single-particle dispersion,  $\varepsilon(k)$ , into cosine and sine harmonics, as given in equation (8). Note that, in contrast to summing  $N$  independent random variables, the large- $N$  limit of the unitary group plays the role of the thermodynamic limit here, yielding an intrinsic variance of order  $m$  rather than vanishing with  $N$ .

This is a direct physical consequence of the fact that the central-limit behavior we exploit here is of a *random-matrix* type rather than the textbook i.i.d. kind. For Haar  $U(N)$ , the random variables  $\text{Tr } U^r$  have  $O(1)$  variances (no  $1/\sqrt{N}$  normalization), different powers become asymptotically independent by unitary orthogonality, and the relevant regularity condition is of Szegő type [18] (summability of  $r(a_r^2 + b_r^2)$ ), not Lindeberg’s. These features lead to error controls

and growth windows (e.g. total-variation CLTs up to  $m(N) = o(N^{2/3})$  and super-exponential accuracy if  $m \ll \sqrt{N}$  [19]) that are quite unlike the Berry–Esseen picture for sums of i.i.d. variables; see also [16] for finite- $N$  trace moments and orthogonality, [17] for the linear statistics CLTs, and the Gibbs lecture by Diaconis [35] for context.

We identify how deviations (non-Gaussian tails) arise when the conditions of the CLT are weakened (multiple slow-decaying modes, symbol singularities, etc.), and we confirm these predictions with both analytic results (Toeplitz determinant asymptotics) and numerical simulations. This Gaussian ‘core’ of the work distribution, with model-specific non-Gaussian tails, suggests clear experimental signatures – e.g. the prevalence of Gaussian statistics in sudden quenches unless the system is tuned to special conditions (long-range interactions or critical points) that produce visible deviations.

Therefore, a natural next step is to drive the system across quantum critical manifolds (or to open boundaries) and ask how the *tails* of the work distribution reorganize. In our mapping, the work characteristic function is the Loschmidt amplitude  $\chi_W(u) = G(-u)$ . When  $G(t)$  develops *Fisher zeros* that approach the real time axis, the strip of analyticity of  $\chi_W(u)$  narrows, and by standard Fourier arguments this slows the decay of  $P(W)$ —revealing structured, non-Gaussian tails. In parallel, when the (block)-Toeplitz symbol acquires *Fisher–Hartwig* features (jumps/zeros) at criticality or at hard edges (OBC), one expects robust algebraic/oscillatory fingerprints in the tails while the *bulk* remains close to Gaussian. Charting these effects side-by-side—within-phase vs across-critical quenches—would provide a clean, experiment-ready test of our Gaussian core with FH/DQPT-controlled tails picture. In particular, we already have computations on the open boundary case with the large  $u$  (tails) asymptotics of the Toeplitz/Hankel determinant evaluated through Painlevé V: the expansion contains explicit power-laws and oscillations that will give non-Gaussian tails controlled by the nearest PV singularity to the real  $u$  axis. This will be discussed elsewhere.

Likewise, by tuning the  $\{a_r\}$  and probing the large-deviation regime of the matrix model (the analogue of Gross–Witten–Wadia transition [4], a third-order phase transition in unitary matrix models, and its multicritical extensions [36]), one can further reorganize the *tails* of  $P(W)$  in universal ways without changing the near-Gaussian bulk—connecting quench thermodynamics to well-studied unitary-matrix universality classes.

## ACKNOWLEDGEMENTS

We thank Gregory Schehr for correspondence.

- 
- [1] S. Deffner and S. Campbell, *Quantum Thermodynamics: An introduction to the thermodynamics of quantum information* (Morgan & Claypool Publishers, 2019).
  - [2] T. Gorin, T. Prosen, T. H. Seligman, and M. Žnidarič, *Physics Reports* **435**, 33 (2006).
  - [3] D. Pérez-García, L. Santilli, and M. Tierz, *Physical Review Research* **6**, 033007 (2024).
  - [4] D. Pérez-García, L. Santilli, and M. Tierz, *Quantum* **8**, 1271 (2024).
  - [5] P. J. Forrester, *Log-gases and random matrices (LMS-34)* (Princeton university press, 2010).
  - [6] D. García-García and M. Tierz, *Journal of Combinatorial Theory, Series A* **172**, 105201 (2020).
  - [7] P. Talkner, E. Lutz, and P. Hänggi, *Physical Review E* **75**, 050102(R) (2007).
  - [8] M. Campisi, P. Hänggi, and P. Talkner, *Reviews of Modern Physics* **83**, 771 (2011).
  - [9] M. Esposito, U. Harbola, and S. Mukamel, *Reviews of Modern Physics* **81**, 1665 (2009).
  - [10] A. Silva, *Physical Review Letters* **101**, 120603 (2008).
  - [11] M. Heyl, A. Polkovnikov, and S. Kehrein, *Physical Review Letters* **110**, 135704 (2013).
  - [12] M. Heyl, *Reports on Progress in Physics* **81**, 054001 (2018).
  - [13] R. Dorner, S. R. Clark, L. Heaney, R. Fazio, J. Goold, and V. Vedral, *Physical Review Letters* **110**, 230601 (2013).
  - [14] L. Mazzola, G. De Chiara, and M. Paternostro, *Physical Review Letters* **110**, 230602 (2013).
  - [15] T. B. Batalhão, A. M. Souza, L. Mazzola, R. Auccaise, I. S. Oliveira, J. Goold, G. De Chiara, M. Paternostro, and R. M. Serra, *Physical Review Letters* **113**, 140601 (2014).
  - [16] P. Diaconis and M. Shahshahani, *Journal of Applied Probability* **31A**, 49 (1994).
  - [17] P. Diaconis and S. N. Evans, *Transactions of the American Mathematical Society* **353**, 2615 (2001).
  - [18] K. Johansson, *Annals of Mathematics* **145**, 519 (1997).
  - [19] K. Johansson and G. Lambert, *The Annals of Probability* **49**, 2961 (2021).
  - [20] M. Duits and K. Johansson, *Transactions of the American Mathematical Society* **362**, 1169 (2010).
  - [21] R. E. Hartwig and M. E. Fisher, *Archive for Rational Mechanics and Analysis* **32**, 190 (1969).
  - [22] K. Zawadzki, A. Kiely, G. T. Landi, and S. Campbell, *Physical Review A* **107**, 012209 (2023).
  - [23] P. Deift, A. Its, and I. Krasovsky, *Annals of mathematics* , 1243 (2011).
  - [24] E. Lieb, T. Schultz, and D. Mattis, *Annals of Physics* **16**, 407 (1961).
  - [25] P. Pfeuty, *Annals of Physics* **57**, 79 (1970).
  - [26] E. Barouch and B. M. McCoy, *Physical Review A* **3**, 786 (1971).
  - [27] N. Onishi and S. Yoshida, *Nuclear Physics* **80**, 367 (1966).
  - [28] L. M. Robledo, *Physical Review C* **79**, 021302 (2009).
  - [29] I. Klich, *Quantum Noise in Mesoscopic Physics* , 397 (2003).
  - [30] E. L. Basor and T. Ehrhardt, *Communications in Mathematical Physics* **234**, 491 (2003).
  - [31] B.-Q. Jin and V. E. Korepin, *Journal of Statistical Physics* **116**, 79 (2004).
  - [32] D. Perez-Garcia and M. Tierz, *Physical Review X* **4**, 021050 (2014).
  - [33] L. Santilli and M. Tierz, *Journal of Statistical Mechanics: Theory and Experiment* **2020**, 063102 (2020).
  - [34] D. Freedman and P. Diaconis, *Zeitschrift für Wahrscheinlichkeitstheorie und Verwandte Gebiete* **57**, 453 (1981).
  - [35] P. Diaconis, *Bulletin of the American Mathematical Society* **40**, 155 (2003).
  - [36] P. Le Doussal, S. N. Majumdar, and G. Schehr, *Physical review letters* **121**, 030603 (2018).

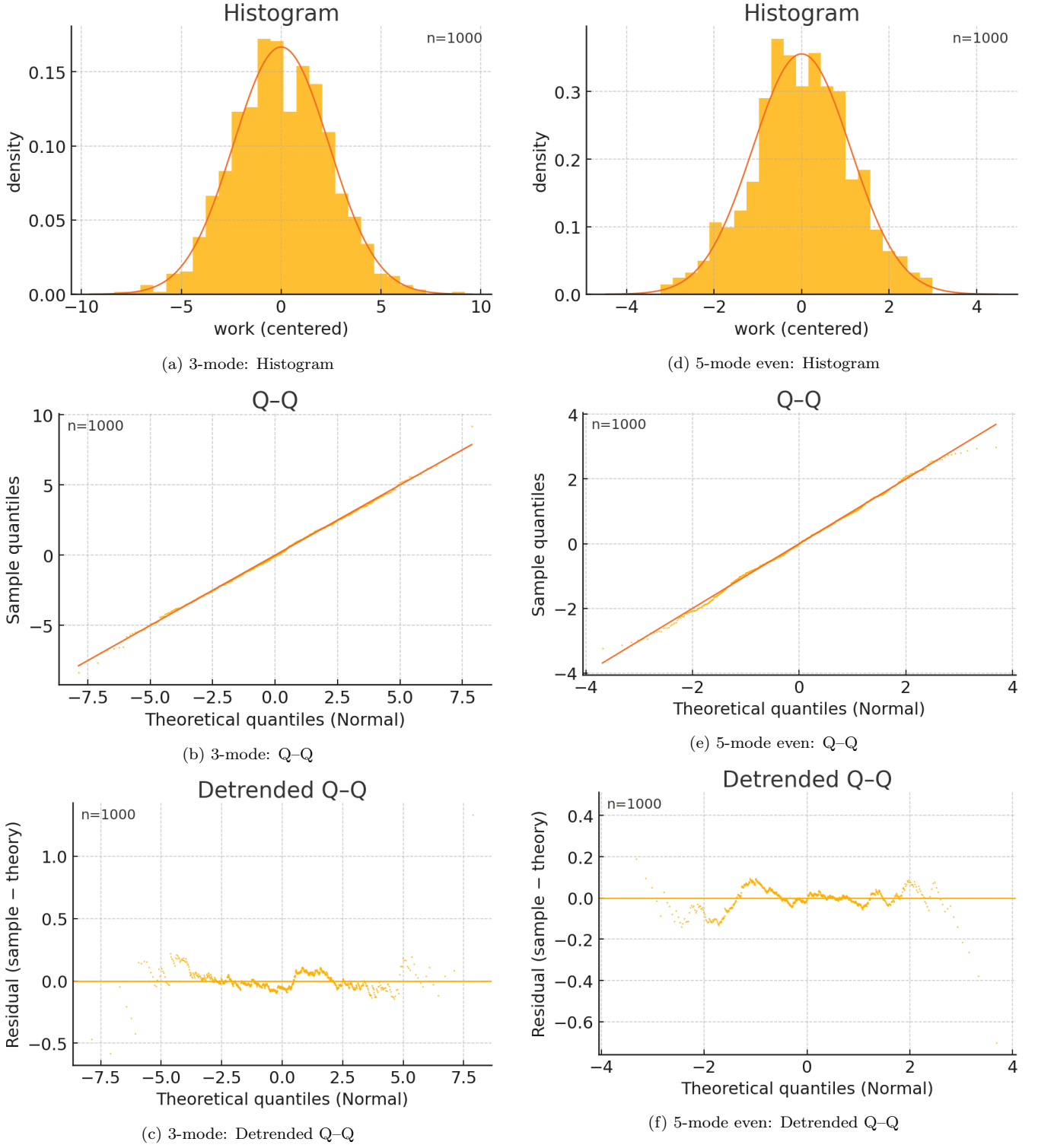
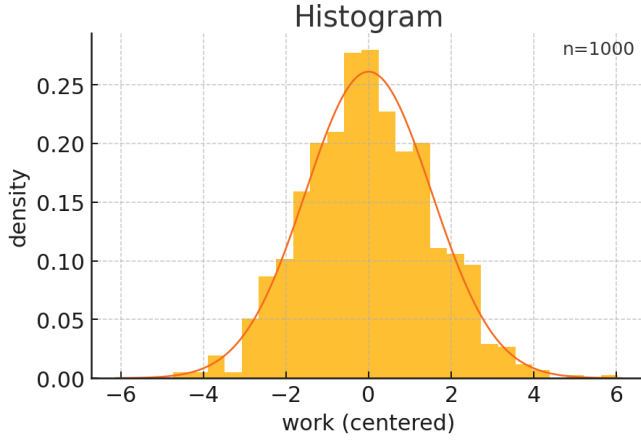
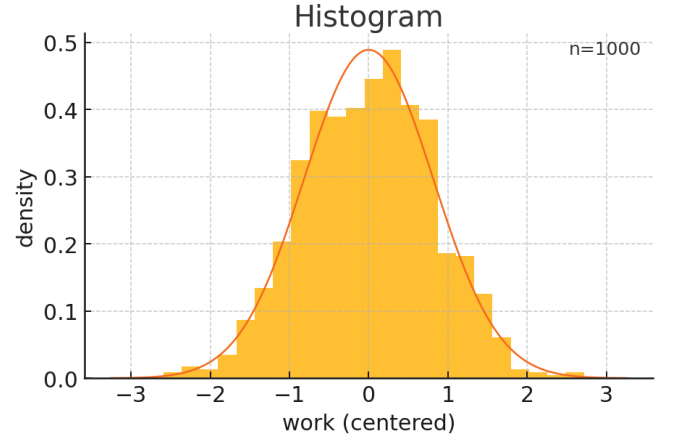


FIG. 1. Side-by-side diagnostics for two families at  $N = 80$ ,  $n = 1000$  samples. Left: 3-mode model  $\mathcal{M} = \{1, 2, 3\}$  with  $\alpha_1 = 1.0, \alpha_2 = 0.7, \alpha_3 = 0.5$ . Right: 5-mode even model  $\mathcal{M} = \{2, 4, 6, 8, 10\}$ ,  $\alpha_m = e^{-0.4m}$ . Each column shows the histogram with Gaussian overlay, the Q-Q plot (points +  $y = x$ ), and the detrended Q-Q (residuals vs theory).

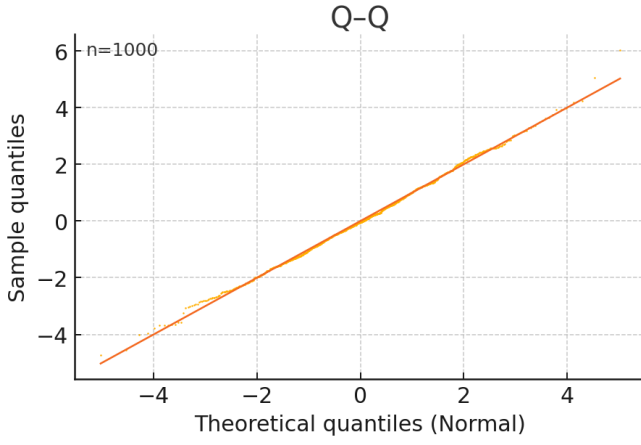




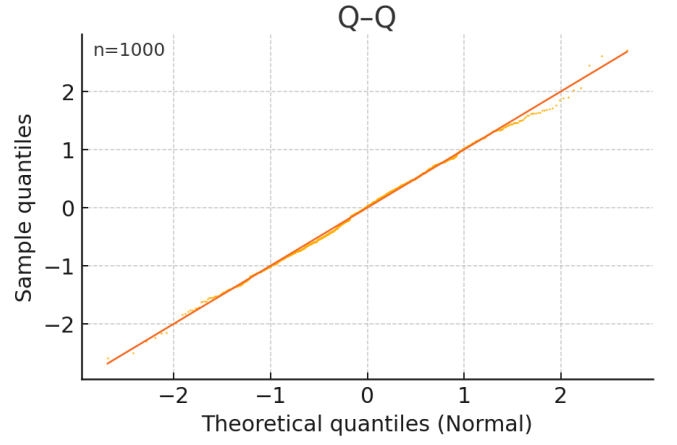
(a) Power-law: Histogram



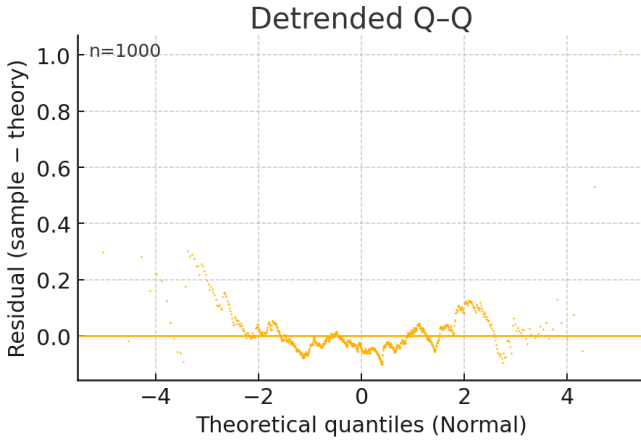
(d) Exponential even: Histogram



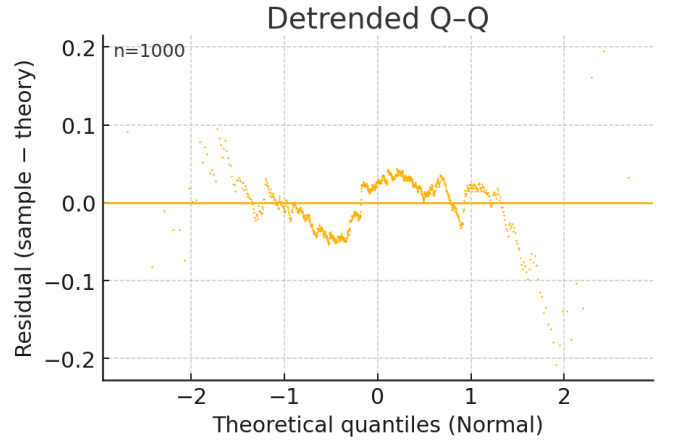
(b) Power-law: Q-Q



(e) Exponential even: Q-Q



(c) Power-law: Detrended Q-Q



(f) Exponential even: Detrended Q-Q

FIG. 2. Diagnostics for power-law (left;  $\alpha_m = m^{-2}$ ) and exponential even (right;  $\alpha_m = e^{-0.5m}$ ) families at  $N = 80$ ,  $n = 1000$  samples.

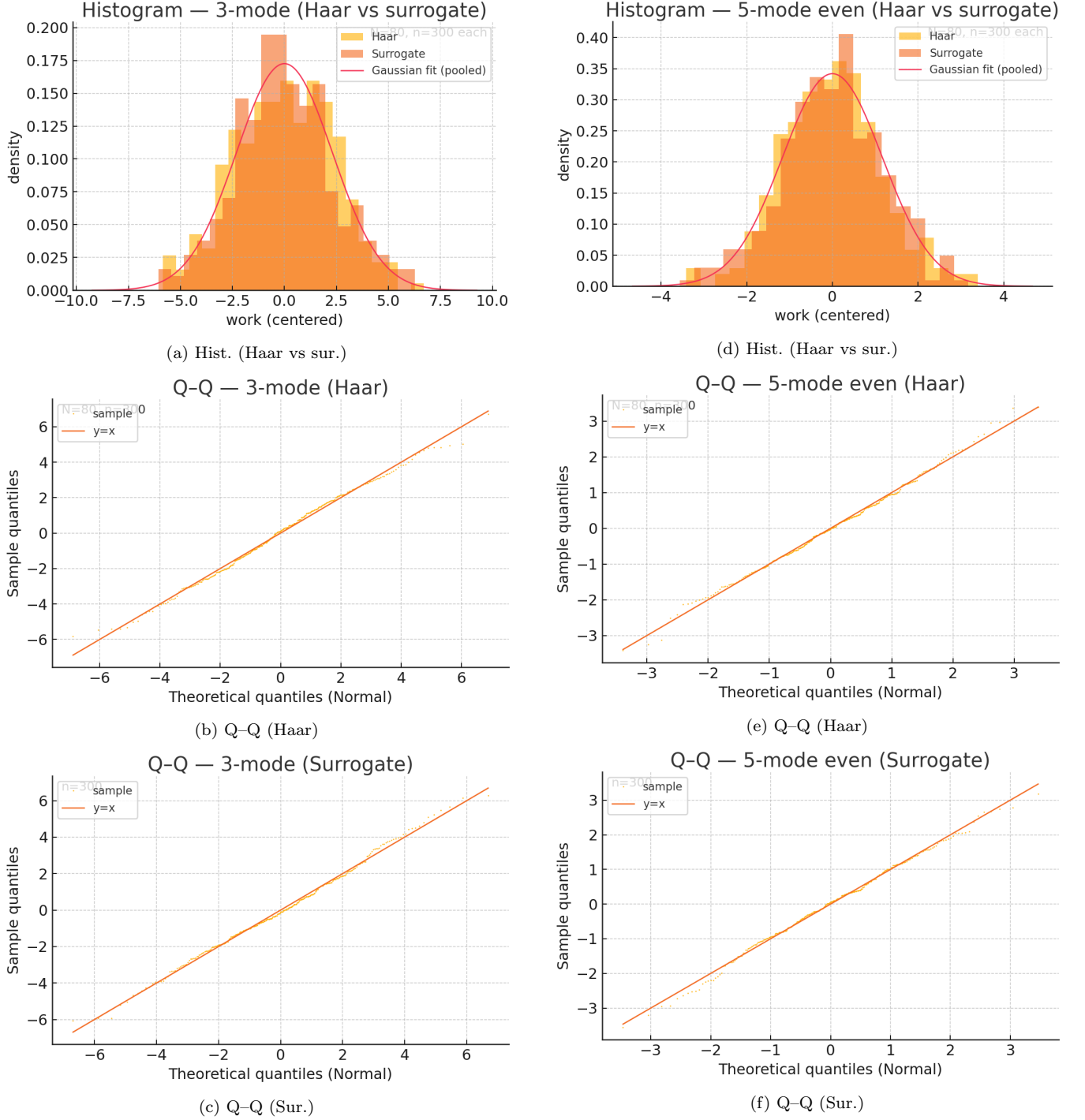


FIG. 3. Surrogate vs exact Haar at  $N = 80$ ,  $n = 300$  per sample. Left: 3-mode  $\mathcal{M} = \{1, 2, 3\}$ ,  $\alpha_1 = 1.0, \alpha_2 = 0.7, \alpha_3 = 0.5$ . Right: 5-mode even  $\mathcal{M} = \{2, 4, 6, 8, 10\}$ ,  $\alpha_m = e^{-0.4m}$ . Rows: (top) histogram overlays (Freedman–Diaconis bins; pooled Gaussian fit), (middle) Q–Q (Haar), (bottom) Q–Q (surrogate).

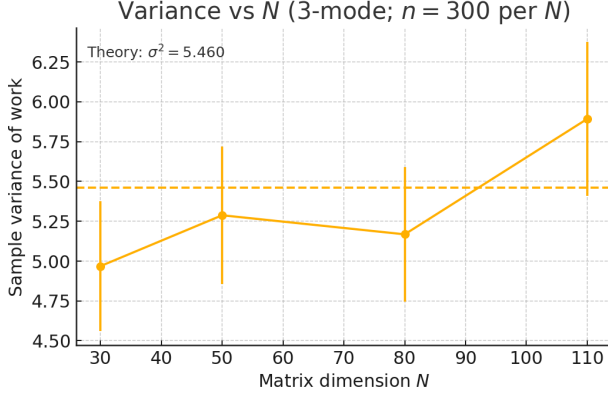
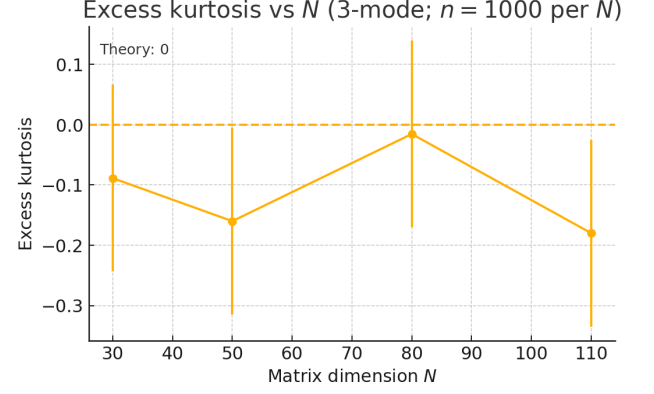
(a) Variance vs  $N$ .(b) Excess kurtosis vs  $N$ .

FIG. 4. Diagnostics across  $N$  for the 3-mode model  $\mathcal{M} = \{1, 2, 3\}$ ,  $\alpha_1 = 1.0$ ,  $\alpha_2 = 0.7$ ,  $\alpha_3 = 0.5$ . (a) Sample variance with analytic prediction (dashed) and SE bars  $\hat{\sigma}^2 \sqrt{2/(n-1)}$  ( $n = 300$  per  $N$ ). (b) Excess kurtosis with baseline error bars  $\sqrt{24/n}$  ( $n = 1000$  per  $N$ ); dashed line marks the Gaussian limit.

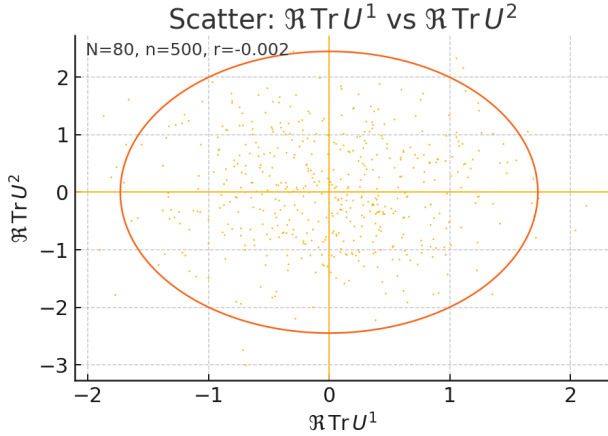
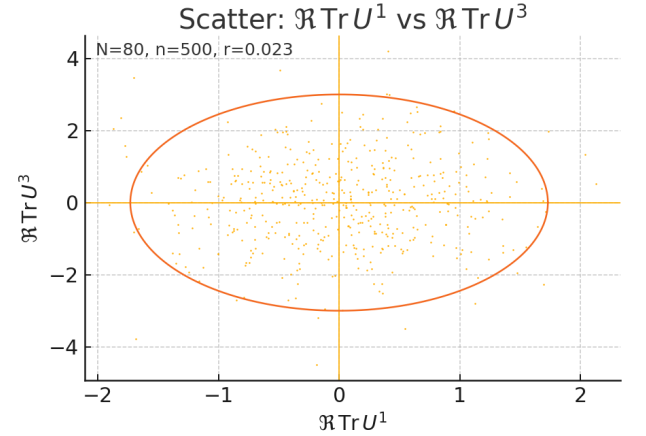
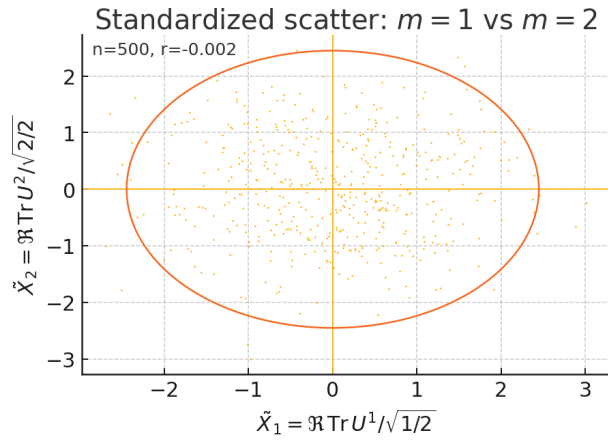
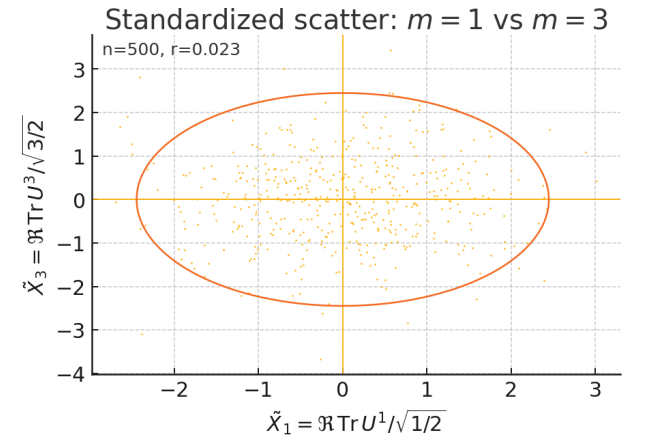
(a)  $\Re \text{Tr } U$  vs  $\Re \text{Tr } U^2$ .(b)  $\Re \text{Tr } U$  vs  $\Re \text{Tr } U^3$ .(c) Standardized:  $m = 1$  vs  $m = 2$ .(d) Standardized:  $m = 1$  vs  $m = 3$ .

FIG. 5. Scatter diagnostics with theory 95% contours (ellipse/circle). Top: raw coordinates show the  $(\sqrt{m/2})$  scale on each axis; bottom: standardized coordinates divide by  $\sqrt{m/2}$  so the 95% contour is a circle, making different  $(m, n)$  pairs directly comparable. Annotations in the panels report the sample correlation  $r$  (theory:  $r = 0$ ); here  $n = 500$  samples.